PAPER

Check for updates

Explosive vapour/particles detection using SERS substrates and a hand-held Raman detector†

Vered Heleg-Shabtai, [ID] *[a] Amalia Zaltsman,[a] Mali Sharon,[a] Hagai Sharabi,[a] Ido Nir,[a] Dana Marder,[b] Guy Cohen,[c] Izhar Ron[a] and Alexander Pevzner [ID] *[a]

We developed and optimized surface-enhanced Raman spectrometry (SERS) methods for trace analysis of explosive vapour and particles using a hand-held Raman spectrometer in the field. At first, limits of detection (LODs) using SERS methods based on a colloidal suspension of gold nanoparticles were measured under alkaline conditions and are as follows: pentaerythrol tetranitrate (PETN) (1.5×10^{-6} M, 6.9 ng), 1,3,5,7-tetranitro-1,3,5,7-tetrazoctane (HMX), 8.1×10^{-6} M, 35 ng; urea nitrate (UN), 9.2×10^{-4} M, 165 ng; 2,4,6-trinitrotoluene (TNT), 1.1×10^{-7} M, 0.35 ng. We developed SERS substrates that demonstrate the wide applicability of this technique for use in the field for explosive vapour and particles adsorbed on a surface based on Au nanoparticles that were optimal for the detection of the target materials in solution. Au nanoparticles were modified onto quartz fibres or a polyurethane sponge for vapour/particles detection. SERS detection of vapours of 2,4-dinitrotoluene (2,4-DNT) and 1,3-dinitrobenzene (1,3-DNB) was shown by sampling vapours onto Au-modified quartz fibres followed by hand-held Raman analysis with estimated minimum detection levels of 3.6 ng and 54 ng, respectively. The detection of 2,4-DNT using sponge-based SERS decorated with Au nanoparticles was also demonstrated; however, the sensitivity was lower than that observed using quartz fibres. The detection of TNT on a surface was performed by utilizing quartz-fibres precoated with alumina and modified with Au nanoparticles, and the detection of 10 μg (0.53 μg cm^{-2}) of TNT was demonstrated.

1. Introduction

Trace detection of explosives is a particularly challenging task owing to the diverse characteristics of explosive materials, such as a wide variety of materials that can be used as explosives, the low vapour pressure of common explosives (approximately 10 ppb for 2,4,6-trinitrotoluene (TNT) and 10 ppt for cyclotrimethylenetrinitramine (RDX) and pentaerythrol tetranitrate (PETN)),[1] and the presence of improvised explosives. Sampling techniques for the trace detection of explosives typically involve collecting vapours or particulate samples and analyzing them using a sensitive sensor-based system. Currently, many different techniques exist for the detection of trace amounts of explosives; the most common include ion mobility spectrometry (IMS) and mass spectrometry (MS).[2,3] Furthermore, colorimetric kits are also in comprehensive use. Surface-enhanced Raman spectrometry (SERS) has become an increasingly useful technique in homeland security applications (chemical and biological threats, and explosive materials).[4,5] Raman spectroscopy provides unique structural information regarding the vibrational spectrum of diverse species.[6] Using an appropriate database and algorithm, this information can be used to identify the contents of a sample. The utilization of Raman spectroscopy with SERS can increase the Raman signal of the target molecule by 6–10 orders of magnitude and therefore significantly increases the sensitivity, allowing the analysis of materials at low concentrations.[7,8]

Hand-held/portable Raman detectors enable on-site detection of solid and liquid samples for homeland security purposes. Using SERS expands the capabilities of gas-phase analysis by initially adsorbing the vapours of the target materials onto a SERS substrate followed by analysis using a hand-held Raman detector.[9–11]

Hakonen *et al.*[12] demonstrated ultra-sensitive detection of RDX and picric acid in the range of 0.8–4 pg using commercially available SERS substrates and a hand-held Raman spectrometer. Jankiewicz *et al.*[13] investigated the detection of trace amounts of selected explosive materials on various commercial and non-commercial SERS substrates using portable Raman instruments. Detection ranged from single to hundreds of μg cm^{-2} was demonstrated, depending on the type of explosive

[a]Department of Physical Chemistry, Israel Institute for Biological Research, P.O. Box 19, Ness-Ziona 74100, Israel. E-mail: veredhs@iibr.gov.il; alexanderp@iibr.gov.il; Fax: +972 89381743; Tel: +972 89381457

[b]Department of Analytical Chemistry, Israel Institute for Biological Research, P.O. Box 19, Ness-Ziona 74100, Israel

[c]Environmental Physics Department, Israel Institute for Biological Research, P.O. Box 19, Ness-Ziona 74100, Israel

(ammonium nitrate, RDX and TNT) and Raman spectrometer (portable/hand-held). Soma et al.[14] demonstrated the capability to detect explosives (picric acid, 3-nitro-1,2,4- triazol-5-one and 2,4-dinitrotoluene) in various mixtures with dyes and other explosives using fabricated SERS substrates and a portable Raman spectrometer. The detection limits obtained in the case of explosive mixtures was in the range of micromolars.

Herein, we demonstrate the detection and identification of various explosive materials using a variety of sampling techniques including swab and gas-phase sampling. Firstly, SERS methods for the detection of PETN, urea nitrate (UN), 1,3,5,7-tetranitro-1,3,5,7-tetrazoctane (HMX), TNT and TNT precursors (Fig. S1†) were developed in a Au colloidal nanoparticle suspension. Secondly, optimized nanoparticles for SERS detection in solution were adsorbed onto quartz fibres or a polyurethane sponge, which were used for wiping surfaces or gas-phase sampling and were then analyzed using a hand-held Raman spectrometer.

2. Experimental

2.1 Chemicals

Hydroxylamine hydrochloride, trisodium citrate, ascorbic acid, hydrogen tetrachloroaurate trihydrate ($HAuCl_4 \cdot 3H_2O$), alumina, sodium hydroxide, pentaerythritol, acetonitrile (AcCN), and methanol (MeOH) were purchased from Sigma-Aldrich. 2,4-dinitrotoluene (2,4-DNT) in MeOH : AcCN (1 : 1) 1 mg mL^{-1}, 1,3-dinitrobenzene (1,3-DNB) in MeOH : AcCN (1 : 1) 1 mg mL^{-1}, 2,6-dinitrotoluene, (2,6-DNT) in MeOH : AcCN (1 : 1) 1 mg mL^{-1}, TNT in MeOH : AcCN (1 : 1) 1 mg mL^{-1}, HMX in MeOH : AcCN (1 : 1) 1 mg mL^{-1}, PETN in MeOH 1 mg mL^{-1}, and urea nitrate (UN) in MeOH : AcCN (1 : 1) 1 mg mL^{-1} were purchased from AccuStandard® (New Haven, CT, USA). Ultrapure deionized water (Barnstead Nanopure system, Dubuque, IA, USA) was used throughout the experiments. Lower concentration solutions of the explosives were prepared by serial dilution in MeOH or MeOH : AcCN (1 : 1) and were stored at 4 °C prior to use.

2.2 Synthesis of colloidal Au nanoparticle suspensions

Colloidal Au nanoparticle suspensions were synthesized via the iterative hydroxylamine seeding method previously described by Brown et al.[15] Briefly, the initial colloidal batch (~12 nm Au colloid nanoparticles) was prepared using the Frens method,[16] via the addition of 38.8 mM of sodium citrate to a stirred solution of boiling 0.01% w/w $HAuCl_4 \cdot 3H_2O$. This mixture was boiled for 15 min and then stirred for an additional 10 min as it cooled. All subsequent colloid suspensions (Au(B–E), Table S1†) were produced by mixing reagent α (0.2 M hydroxylamine hydrochloride) with the diluted colloidal suspension in water and then adding reagent β (1.0% w/w $HAuCl_4 \cdot 3H_2O$ solution) to initiate the reaction. After adding reagent β, the colloidal suspension was stirred vigorously for 10 min at room temperature. The quantities of the reagents used for subsequent growth of the colloidal suspensions are summarized in Table S1.† After preparation, all colloidal suspensions were stored at 4 °C until further use.

Colloidal Au nanoparticle suspensions for UN detection were synthesized using the method previously described by Murphy et al. with some modifications.[17] The initial colloidal batch (~12 nm Au colloid nanoparticles) was prepared as described above. 150 μL of 12 nm Au seeds with 2.5 mL $HAuCl_4 \cdot 3H_2O$ 10 mM were diluted up to 150 mL with deionized water. Under continuous stirring of the solution, 100 mL of freshly prepared ascorbic acid 4×10^{-4} M was added slowly at a flow rate of 10 mL min^{-1}. After preparation, the colloidal suspensions (Au–Asc) were stored at 4 °C.

2.3 Fibre/sponge-based SERS substrates

Quartz fibre-based SERS substrates were prepared using a simple drop casting method. Initially, Whatman® quartz filters (CAT no. 1851-047) were cut into pieces approximately 1.0 × 1.5 cm^2 in size. Then an approximately 200 μL Au colloidal nanoparticle suspension was uniformly added dropwise onto two layers of the cut filters.[18,19] After air drying the filters (approximately 10 min), the coating procedure was repeated a further nine times. For wiping surface purposes, the quartz filter pieces were dipped into an alumina suspension in water (1% w/w) for 1 min prior to the deposition of the Au nanoparticles.[20]

The sponge-based SERS substrates were prepared using the immersion deposition method. The polyurethane soft foam (SF) sponge was cut into 10 × 8 mm pieces. The pieces of polyurethane SF sponge were immersed for several hours in the Au–E colloidal nanoparticle suspension and the suspension was replaced twice.

After preparation the fibre/sponge-based SERS substrates were dried and stored at 4 °C until further use.

2.4 SERS substrate (suspension and fibres/sponge-based) characterization

The size and shape of the colloidal Au nanoparticle suspensions were characterized using UV-vis spectroscopy and scanning/transmission electron microscopy (SEM/TEM) analyses. UV-vis spectra of the Au suspensions were acquired using a Shimadzu UV-2401 dual-beam spectrophotometer equipped with halogen and deuterium lamps (190–900 nm range), and a resolution of 0.1 nm. For the TEM analysis, the Au suspensions were applied to 400 mesh formvar/carbon-coated copper grids. The samples were incubated for 0.5 min and the excess liquid was carefully blotted with Kimwipe® paper. After air drying, the samples were imaged using an FEI Tecnai T-12 transmission electron microscope operated at 120 kV and equipped with a Gatan ES500 W Erlangshen camera.

Analysis of the Au colloids modified onto quartz fibres and the polyurethane SF sponge were performed using an FEI Quanta 200 field emission gun (FEG) environmental scanning electron microscope (ESEM). Images of the quartz fibre-based SERS substrates were obtained at 20 kV under low vacuum conditions. Images of the polyurethane SF sponge were obtained at 10 kV after 5 nm iridium sputter coating. The sputter coating was performed using a Q150T Quorum sputter coater.

2.5 Raman measurements using the nanoparticle suspension

Raman spectra were collected using a FirstDefender™ hand-held Raman spectrometer (ThermoFisher Scientific, Inc.). Excitation was provided by a 785 nm diode laser with an output power of 300 mW. The Raman measurements of the samples using the nanoparticle suspension were performed in glass vials that were 1.46 cm in diameter using the FirstDefender vial holder. The accumulation time ranged from 0.25 to 10 s. Explosives with defined concentrations were added to 1 mL of the Au colloidal suspension, followed by the addition of NaOH solution. Alkaline conditions produce a significant enhancement in the SERS signal strength.[21,22] Prior to the Raman measurements the samples were vortexed. The optimized procedure and method for the detection of various explosive materials is summarized in Fig. S2(A)† and Table 1. The optimized SERS methods in the nanoparticle suspension served as a basis for the on-site sampling and SERS detection.

2.6 SERS measurements from wiped surfaces

Explosive at known concentrations were dropped onto glass slides (2.5 × 7.5 cm^2) and air-dried. Afterwards, the slides were wiped with quartz fibre-based SERS substrates (alumina-coated) that had been previously wetted with a solution of AcCN : MeOH (1 : 1). After sampling, 40 μL NaOH 0.5 M was dropped onto the SERS substrates and Raman measurements were performed in the shoot mode by focusing the laser beam at an approximate distance of 3 mm (using the position cone) from the surface, Fig. S2(B).†

2.7 Experimental setup for gas-phase measurements

Exposure of the quartz/sponge-based SERS substrate to 2,4-DNT and 1,3-DNB (volatile TNT precursors) was performed using a homemade gas-phase flow system that has been previously described by Gura et al.[23] An inert HP-6890 GC split/splitless injector was equipped with a homemade liner packed with Carbofrit and a 10 cm interface DB5-MS column with a 0.25 mm internal diameter and a 0.1 μm film thickness (cut from a 15 m column, CAT no. 122.5511, Agilent). The injector temperature was maintained at 225 °C with an N$_2$ flow rate of 4 mL min^{-1}. To generate a known vapour concentration, 2 μL of TNT precursors of known concentrations were injected into the pre-heated injection port for complete and efficient evaporation. The injections were performed while the short-interface DB5-MS column was inserted 1 cm inside the sampling tube and pumping at a constant flow rate of 200 mL min^{-1} for 5 min, see
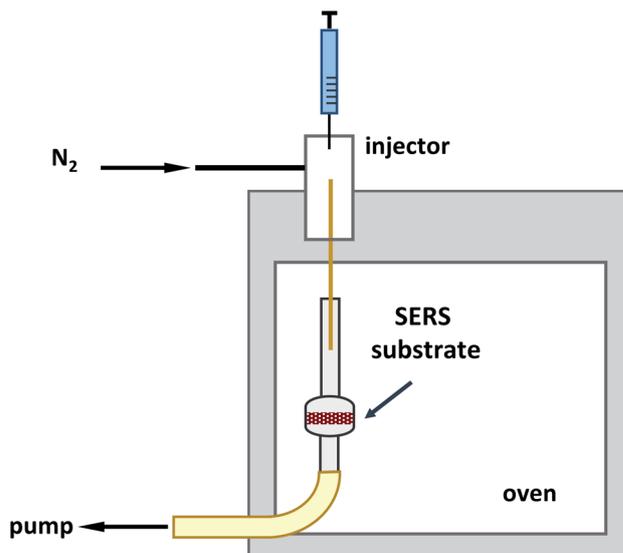

Fig. 1 Schematic diagram of the vapor source setup based on an inert gas chromatography inlet.

Fig. 1. Prior to vapour exposure, the quartz/sponge-based SERS substrates were wetted using a few drops of NaOH 1 M. For the quartz-based substrates, the Raman measurements were performed in the shoot mode by focusing the laser beam at an approximate distance of 3 mm (using the position cone) from the surface, Fig. S2(C).† Raman measurements using the sponge-based SERS substrates were performed in vials filled with water, in order to prevent localized heating of the sponge by the laser beam, which can produce smoke, Fig. S2(D).†

3. Results and discussion

3.1 Characterization of the colloidal suspension and quartz/sponge-based substrates

Colloidal Au nanoparticle suspensions were synthesized using the iterative hydroxylamine seeding method[15,16] and characterized using UV-vis and electron microscopy. The wavelength λ_{max} (maximum absorbance) was red-shifted from 519 to 530 nm for Au–D nanoparticles and to 536 nm for Au–E nanoparticles as a result of the increase in the size of the nanoparticles, Fig. S3.†[24] TEM images of the Au–D and Au–E nanoparticles, which have an almost spherical shape and an average diameter of 44 ± 8 and 60 ± 5 nm, respectively, are shown in Fig. S4.† An SEM image of the Au–Asc nanoparticles with an average diameter of 75 ± 10 is shown in Fig. S5.†

Table 1 Optimized SERS methods for the detection of explosives in nanoparticle suspension

Target material	Colloidal suspension	Alkaline condition	Notes
PETN	Au–E	NaOH 10 mM	Prior to NaOH addition, 20 μL of MeOH was added
HMX	Au–D	NaOH 200 mM	
TNT/2,4-DNT/2,6-DNT/1,3-DNB	Au–D	NaOH 36 mM	
UN	Au–Asc	NaOH 28 mM	

From the preliminary studies used to analyze the dependence of the SERS intensity on the nanoparticle properties (including type of metal, surface coverage and size) in suspension, it was found that the above-mentioned nanoparticles provide a relatively high performances.

Fig. 2A and B show photographs of the quartz fibre filter and polyurethane SF sponge decorated with Au nanoparticles, which were utilized as a SERS substrate for vapour analysis of TNT precursors. For particulate analysis on a surface, quartz fibres precoated with alumina were modified with Au nanoparticles and used for wiping the surfaces, see Fig. 2C. The SEM back scattered electron (BSE) images of the decorated typical quartz fibres (without and with alumina) and a polyurethane SF sponge are shown in Fig. 2D–F. The Au nanoparticle clusters decorating the quartz fibres and polyurethane SF sponge can be clearly observed. These clusters provide the localized surface plasmon resonance that leads to a large SERS enhancement owing to the formation of hot spots.[25]

3.2 SERS detection of explosives in nanoparticle suspension

The initial SERS methods used for the detection of PETN, UN, HMX, TNT and TNT precursors were developed in nanoparticle suspension. These methods served as a basis for the follow-up stage for the analysis of gas-phase and surface-deposited particles. For suspension-based detection, all Raman measurements were performed in glass vials. The limits of detection (LODs) of the target materials and the minimal detectable masses in suspension were determined. The LOD was defined as the concentration at which the signal level of the substance reached a level that was at least three times the signal noise of the baseline.

3.2.1 SERS detection of PETN in nanoparticle suspension.
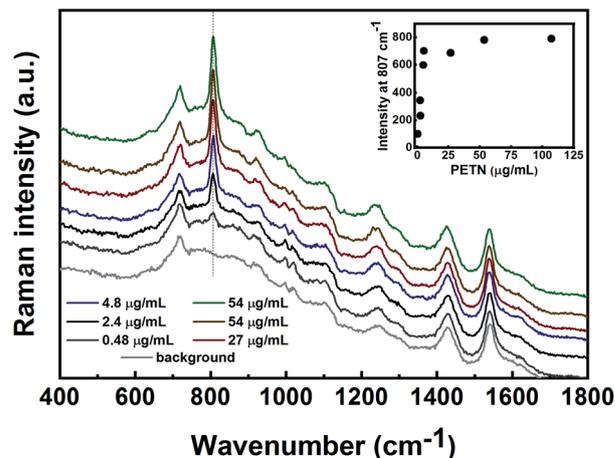In general, the normal Raman (NR) spectrum of PETN is

Fig. 3 PETN SERS spectra at several concentrations using Au–E nanoparticle suspensions under alkaline conditions (NaOH 10 mM) and an accumulation time of 5 s. Inset shows the SERS intensity at 807 cm^{-1} *versus* the PETN concentration.

characterized by major Raman bands at 1290 cm^{-1} (symmetric NO_2 stretching), 871 cm^{-1} (symmetric ON stretching) and 622 cm^{-1} (CCC banding).[26] The SERS spectra at several concentrations of PETN was achieved using an Au–E nanoparticle suspension, under alkaline conditions, as shown in Fig. 3. Addition of NaOH is essential to receive the SERS spectra. In the PETN SERS spectra, the major band is located at 807 cm^{-1}. Owing to the dissimilarity between the NR and SERS spectra, it can be assumed that the typical SERS spectrum of PETN under alkaline conditions is related to the hydrolyzed product pentaerythritol or the pentaerythritol nitro residues.[27] The NR spectrum of pentaerythritol is characterized by three bands at 873 cm^{-1} (CH$_2$ rocking), 439 cm^{-1} (CCC banding), and
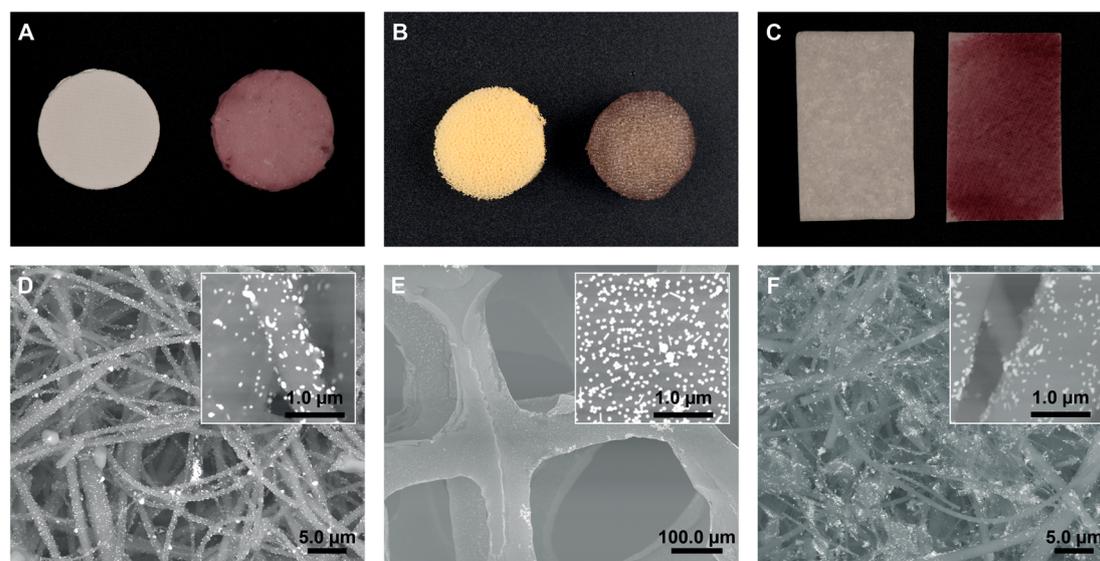

Fig. 2 Photographs of the SERS substrates before and after decoration with Au nanoparticles: (A) quartz fibers; (B) polyurethane sf sponge; and (C) quartz fibers precoated with alumina. SEM BSE images of typical decorated SERS substrates: (D) quartz fibers; (E) polyurethane sf sponge; and (F) quartz fibers precoated with alumina.

the dominant band at 810 cm^{-1} (CH$_2$ rocking), as shown in Fig. S6.†[26] The LOD for PETN detection in solution was found to be 0.48 μg mL^{-1} (1.5 × 10^{-6} M). The intensity of the peak at 807 cm^{-1} was plotted *versus* the PETN concentration and is shown in the inset in Fig. 3. As expected, the signal response over this concentrations range is nonlinear. At low concentrations, the SERS intensity increases linearly with the concentration. As the concentration of the analyte is increased further, the response curve reaches a plateau owing to the surface saturation and multilayer build-up.[28] To estimate the minimum detectable mass of PETN, the effective excitation volume (V) was calculated using the equation for the volume of a cylinder: $V = \pi(d/2)^2 h$, in which d is the equivalent diameter of the laser spot (1.8 mm) and h is the estimated penetration depth of the laser beam (5.75 mm, half of the inner vial diameter), as shown in Fig. S7.† The effective excitation volume (V) was calculated and found to be 14.6 mm^3 (1.46 × 10^{-5} L), and the estimated minimum detectable mass ($m = C \times V \times M_w$) was found to be approximately 6.9 ng (C is the LOD concentration of the PETN solution and M_w is a molar mass of PETN, 316.14 g mol^{-1}).

3.2.2 SERS detection of HMX in nanoparticle suspension.

The SERS spectra at several concentrations of HMX was obtained using the Au–D nanoparticle suspension, under alkaline conditions, as shown in Fig. 4. Addition of NaOH is essential to receive the SERS spectra. The HMX SERS spectra are characterized by a major band at 749 cm^{-1} and an additional minor peak at 842 cm^{-1}. The bands at 749 and 842 cm^{-1} are assigned to the NO$_2$ wagging vibration and NC$_2$ symmetric stretching, respectively.[29] The LOD for HMX detection in solution was found to be 2.4 μg mL^{-1} (8.1 × 10^{-6} M). The intensity of the peak at 749 cm^{-1} was plotted *versus* the HMX concentration in the inset of Fig. 4. As described above, the intensities of the peaks at 749 cm^{-1} increase linearly with the increasing analyte concentration. As the concentration of the analyte is increased further, the response curve reaches a plateau. The estimated minimum detectable mass of HMX is 35 ng (calculated using the same method as described for PETN).
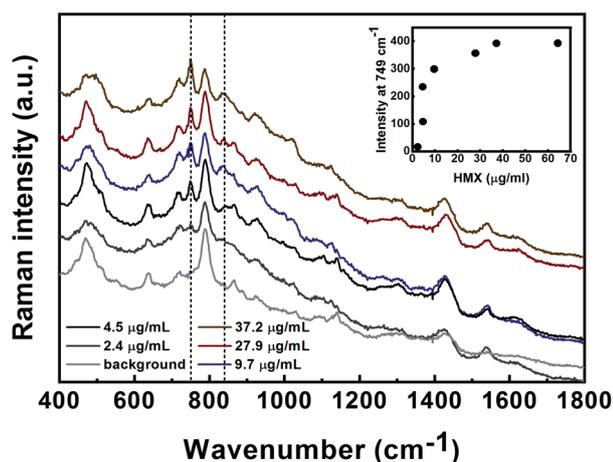
3.2.3 SERS detection of UN in nanoparticle suspension.

In general, the UN Raman spectrum is characterized by a major band at 1050 cm^{-1} (symmetrical stretching vibration of the NO$_3^-$ ion) and minor bands at 1020 cm^{-1} (CN symmetric stretch), 740 cm^{-1} and 722 cm^{-1} (NO$_3^-$ in-plane bending), 572 cm^{-1} (NCO deformation) and 535 cm^{-1} (CN deformation).[30,31] The SERS spectra at several concentrations of UN was obtained using Au–Asc, under alkaline conditions, as shown in Fig. 5. Addition of NaOH is essential to receive the SERS spectra. As the NR and SERS spectra did not correlate, we can assume that under alkaline conditions UN is hydrolyzed to urea, which is sequentially mainly hydrolyzed to carbamic acid, Fig. S8.†[32,33] Therefore, the major band at 611 cm^{-1} in the SERS spectra is assigned to the in-plane deformation of the C=O bond in the primary amides.[34,35] The bands at 685 and 1373 cm^{-1} are assigned to the COO$^-$ deformation and symmetrical stretching, respectively.[36] The LOD for UN detection in solution was found to be 113 μg mL^{-1} (9.2 × 10^{-4} M). The intensity of the peak at 611 cm^{-1} was plotted *versus* the UN concentration and is shown in the inset of Fig. 5. As can be seen, the SERS intensity at 611 cm^{-1} increases with the increasing analyte concentration. The estimated minimum detectable mass of UN is 165 ng (calculated using the method described above for PETN and HMX).

3.2.4 SERS detection of TNT in nanoparticle suspension.

The SERS spectra at several concentrations of TNT was obtained using Au–D, under alkaline conditions, as shown in Fig. 6. Alkaline conditions significantly enhance the SERS signal's strength, therefore improving the LOD by 200. Two major bands observed in the SERS spectra at 1316 and 714 cm^{-1} are assigned to the symmetric NO$_2$ stretching and CCC in-plane ring banding deformation, respectively.[29,37,38] The LOD for TNT detection in solution was found to be 0.024 μg mL^{-1} (1.1 × 10^{-7} M). The intensity at 1316 cm^{-1} was plotted *versus* the sample concentration and is shown in the inset of Fig. 6. A typical profile for the saturation behavior was obtained for the SERS intensity,
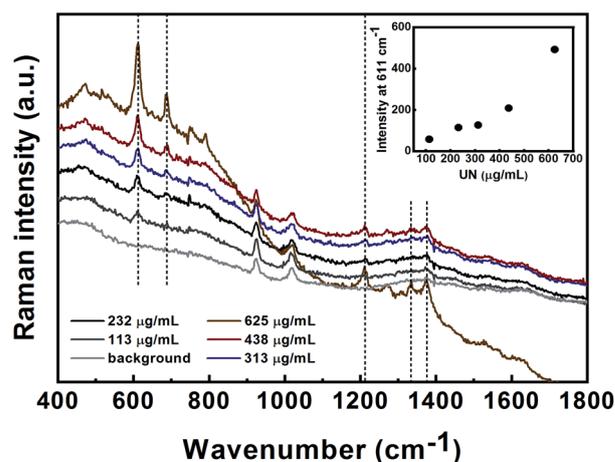

Fig. 4 HMX SERS spectra at several concentrations using the Au–D nanoparticle suspensions under alkaline conditions (NaOH 200 mM) and an accumulation time of 10 s. Inset shows the SERS intensity at 749 cm^{-1} *versus* the HMX concentration.

Fig. 5 UN SERS spectra at several concentrations using Au–Asc nanoparticle suspensions under alkaline conditions (NaOH 28 mM) and an accumulation time of 10 s. Inset shows a graph of the SERS intensity at 611 cm^{-1} *versus* the UN concentration.
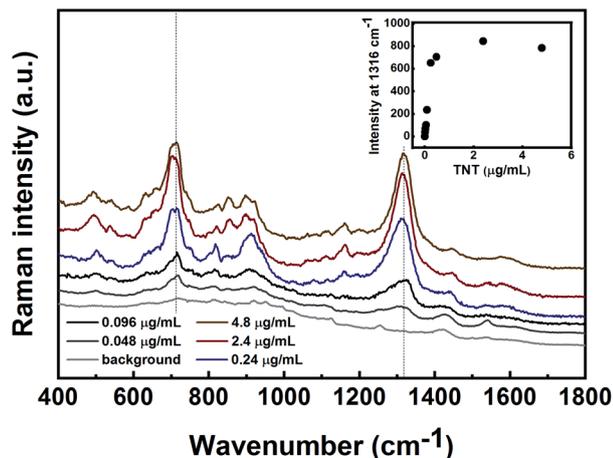
Fig. 6 TNT SERS spectra obtained at several concentrations using Au–D nanoparticle suspensions, under alkaline conditions (NaOH 36 mM) and an accumulation time of 1 s. Inset shows the SERS intensity at 1316 cm^{-1} *versus* the TNT concentration.

which was dependent on the analyte concentration. The estimated minimum detectable mass of TNT is 0.35 ng (calculated using the method described above).

TNT can be indirectly detected by analyzing its volatile impurities.[39] The SERS spectra of 2,4-DNT, 1,3-DNB and, 2,6-DNT in nanoparticle suspension are presented in Fig. S9.† All of the spectra were characterized by the symmetric vibration of the NO$_2$ group in the range of 1316 to 1334 cm^{-1} and the typical vibration of the CNO in the range of 712 to 733 cm^{-1}. For the 1,3-DNB SERS spectrum, a unique aromatic ring breathing mode occurs in the 1000 cm^{-1} region.[40]

3.3 SERS detection of explosives in the field

Detection of hazardous materials using hand-held/portable detectors should be capable of handling a wide variety of matrices and sampling techniques, including swab and gas-phase sampling. SERS was proved to have the potential to serve as a "sniffer" for several target materials including explosives and their precursors, as well as swabs for the detection of adsorbed materials on a surface.[40] To simulate the real-world and to demonstrate the capabilities of the SERS technique for the detection of explosives in the field, we developed a SERS substrate for various applications in field detection.[9] Quartz fibres precoated with alumina and gold nanoparticles served as swabs for the detection of TNT from a surface. For the detection of the volatile precursors of TNT, 2,4-DNT and 1,3-DNB in the gas-phase, quartz fibres and a polyurethane SF sponge decorated with gold nanoparticles were used.

3.3.1 SERS detection of TNT on a surface. Detection of low volatility explosive materials is mainly based on wiping surfaces and performing trace analysis. Herein, we demonstrate the sampling of TNT from a glass surface using a SERS substrate that is based on quartz fibres that were immersed in alumina prior to the modification of the Au nanoparticles on the fibres. Alumina was used to increase the density of the nanoparticles on the upper layers of the surface as it reduces the pore sizes

between quartz yarns, thus increasing the contact area between the nanoparticles and the wiped target material. The color of the alumina-coated quartz fibres decorated with Au nanoparticles (Fig. 2C) is much more intense than the color of the Au modified quartz fibres without an alumina coating (Fig. 2A), which is indicative of the high concentration of Au nanoparticles upon the surface. The SERS spectra of TNT that was wiped from a glass surface (2.5 × 7.5 cm^2) using alumina-coated quartz fibres decorated with Au–E nanoparticles, are shown in Fig. 7. Similar to the TNT SERS spectra in the colloidal suspension, the spectra were characterized using two bands at 1316 cm^{-1} (symmetric NO$_2$ stretching), and 714 cm^{-1} (CCC in-plane ring banding deformation). A typical profile behavior was observed for the SERS intensity at 1316 cm^{-1} which was dependent on the quantity of the analyte, as shown in the inset in Fig. 7. The LOD for TNT detection using surface wipe sampling was found to be 10 μg (the estimated surface concentration of TNT was 0.53 μg cm^{-2}).

3.3.2 SERS detection of TNT precursors in the gas-phase. Detection of the vapours of TNT is limited owing to its low vapour pressure. Therefore detection of TNT based on its volatile impurities including 2,4-DNT, 2,6-DNT and 1,3-DNB, which are characterized by vapour pressures that are at least two orders of magnitude higher, is preferable.[41,42]

Quartz fibres/sponge-based SERS substrates were exposed to vapours of 2,4-DNT or 1,3-DNB in a homemade gas-phase flow system, followed by Raman measurements. Prior to gas-phase exposure, the substrates were slightly wetted using 1 M NaOH.

The SERS spectra of 2,4-DNT and 1,3-DNB obtained using Au decorated quartz fibres are shown in Fig. 8A and B. The spectra of 2,4-DNT and 1,3-DNB are characterized by strong bands at 1316 and 1336 cm^{-1}, respectively, that are assigned to the NO$_2$ symmetric stretching mode. Two other bands at 829 and 1141 cm^{-1} in 2,4-DNT spectra are assigned to the out of plane NO$_2$ mode and the methyl HCH asymmetric band,
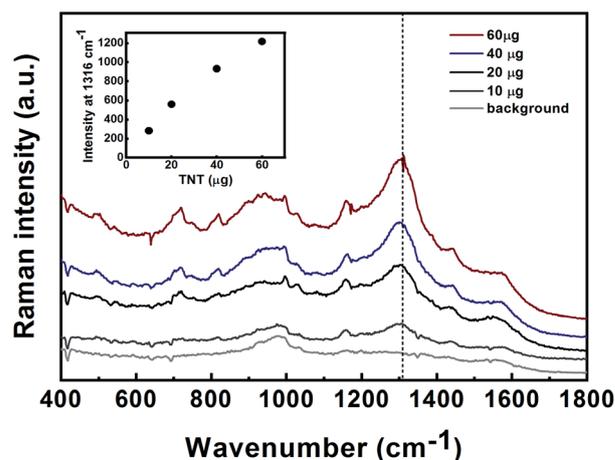

Fig. 7 TNT SERS spectra obtained at several concentrations using alumina-coated quartz fibers decorated with Au–E nanoparticles using an accumulation time of 5 s under alkaline conditions (NaOH 0.5 M). Inset shows a graph of the SERS intensity at 1316 cm^{-1} *versus* the quantity of TNT.
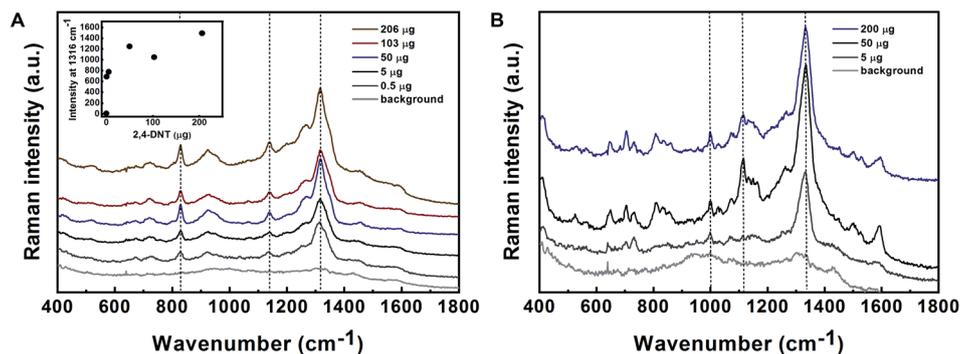
Fig. 8 Gas-phase SERS spectra of 2,4-DNT (A) and 1,3-DNB (B) obtained using au decorated quartz fibers under alkaline conditions and an accumulation time of 5 s. Inset shows a graph of the SERS intensity at 1316 cm^{-1} as a function of the quantity of 2,4-DNT.

respectively.[38] In the inset in Fig. 8A the intensity of 1316 cm^{-1} was plotted *versus* the quantity of 2,4-DNT in the sample. A typical profile for the saturation behavior was observed. The SERS spectra of 1,3-DNB are characterized by a unique aromatic ring breathing mode at 1000 cm^{-1}.[40] The estimated minimal detectable masses of 2,4-DNT and 1,3-DNB in the gas-phase, defined as the concentration at which the signal level of the substance reaches at least three times the signal noise of the baseline, are 0.1 μg and 1.5 μg, respectively. Taking into consideration the effective exposure area (*A*) of the SERS substrate, the 100% vapour adsorption efficiency, and the laser spot size (diameter of 1.8 mm), the minimum detectable masses are estimated to be approximately 3.6 ng and 54 ng for 2,4-DNT and 1,3-DNB, respectively. We assume that the adsorption efficiency is much lower than 100%, therefore the calculated minimum detectable masses are even lower.

We further characterized the vapour detection of 2,4-DNT using sponge-based SERS decorated by Au nanoparticles. The SERS spectra are shown in Fig. S10.† The spectra are characterized by a typical strong band at 1316 cm^{-1} that is assigned to the NO$_2$ symmetric stretching mode. The sensitivity obtained using a sponge was much lower ($\sim$2.5 orders of magnitude) than that obtained using the quartz fibres owing to the large surface area of the sponge and the low localized concentration of the adsorbed target materials upon the surface as a result.

DNT and 1,3-DNB). SERS detection of the vapours of 2,4-DNT and 1,3-DNB was shown by sampling vapours using Au-modified quartz fibres and performing direct analysis of the target materials with estimated minimum detected levels of 3.6 ng and 54 ng, respectively. Detection of 2,4-DNT using sponge-based SERS decorated with Au nanoparticles was also demonstrated; however, the sensitivity was lower than that obtained using quartz fibres. Detection of TNT on a surface was demonstrated by utilizing quartz-fibres precoated with alumina and modified using Au nanoparticles. The detection of 10 μg (0.53 μg cm^{-2}) of TNT was demonstrated. This study shows the development of a SERS technique using sponge/quartz-based SERS substrate that enabled the use of Raman technology for on-site detection of explosives for diverse applications as previously demonstrated for the detection of chemical warfare agents.[9]

Conflicts of interest

There are no conflicts to declare.

Acknowledgements

4. Conclusions

The development of SERS methods (types of nanoparticles and different conditions) in nanoparticle suspension and the modification of these nanoparticles onto quartz fibres or a polyurethane sponge as a sample collector can enable trace particle and vapour detection for homeland security applications. We developed an optimized SERS method for the detection of several explosive materials in solution using a suspension of nanoparticles as a SERS substrate, and achieved the following LODs: PETN, 1.5×10^{-6} M, 6.9 ng; HMX, 8.1×10^{-6} M, 35 ng; UN 9.2×10^{-4} M, 165 ng; TNT, 1.1×10^{-7} M, 0.35 ng, Table S2.† The applicability of the SERS substrates in field detection (vapours and particulate materials) was demonstrated for the detection of TNT and its precursors (2,4-

References

1 R. G. Ewing, M. J. Waltman, D. A. Atkinson, J. W. Grate and P. J. Hotchkiss, *TrAC, Trends Anal. Chem.*, 2013, **42**, 35–48.
2 J. S. Caygill, F. Davis and S. P. J. Higson, *Talanta*, 2012, **88**, 14–29.
3 K. C. To, S. Ben-Jaber and I. P. Parkin, *ACS Nano*, 2020, **14**, 10804–10833.
4 A. Hakonen, P. O. Andersson, M. Stenbæk Schmidt, T. Rindzevicius and M. Käll, *Anal. Chim. Acta*, 2015, **893**, 1–13.
5 F. Yan and T. Vo-Dinh, *Sens. Actuators, B*, 2007, **121**, 61–66.
6 R. S. Das and Y. K. Agrawal, *Vib. Spectrosc.*, 2011, **57**, 163–176.
7 A. I. Pérez-Jiménez, D. Lyu, Z. Lu, G. Liu and B. Ren, *Chem. Sci.*, 2020, **11**, 4563–4577.

8   E. L. Izake, *Forensic Sci. Int.*, 2010, **202**, 1–8.

9   V. Heleg-Shabtai, H. Sharabi, A. Zaltsman, I. Ron and A. Pevzner, *Analyst*, 2020, **145**, 6334–6341.

10 K. B. Biggs, J. P. Camden, J. N. Anker and R. P. V. Duyne, *J. Phys. Chem. A*, 2009, **113**, 4581–4586.

11 M. Lafuente, D. Sanz, M. Urbiztondo, J. Santamaría, M. P. Pina and R. Mallada, *J. Hazard. Mater.*, 2020, **384**, 121279.

12 A. Hakonen, K. Wu, M. Stenbæk Schmidt, P. O. Andersson, A. Boisen and T. Rindzevicius, *Talanta*, 2018, **189**, 649–652.

13 M. Liszewska, B. Bartosewicz, B. Budner, B. Nasiłowska, M. Szala, J. L. Weyher, I. Dzięcielewski, Z. Mierczyk and B. J. Jankiewicz, *Vib. Spectrosc.*, 2019, **100**, 79–85.

14 C. Byram, S. S. B. Moram and V. R. Soma, *Analyst*, 2019, **144**, 2327–2336.

15 K. R. Brown, D. G. Walter and M. J. Natan, *Chem. Mater.*, 2000, **12**, 306–313.

16 G. FRENS, *Nat. Phys. Sci.*, 1973, **241**, 20–22.

17 N. R. Jana, L. Gearheart and C. J. Murphy, *Chem. Mater.*, 2001, **13**, 2313–2322.

18 W. Ma and Y. Fang, *J. Colloid Interface Sci.*, 2006, **303**, 1–8.

19 D. Wu and Y. Fang, *J. Colloid Interface Sci.*, 2003, **265**, 234–238.

20 A. S. L. Lee and Y.-S. Li, *J. Raman Spectrosc.*, 1994, **25**, 209–214.

21 J. I. Jerez-Rozo, O. M. Primera-Pedrozo, M. A. Barreto-Cabán and S. P. Hernández-Rivera, *IEEE Sens. J.*, 2008, **8**, 974–982.

22 J. M. Sylvia, J. A. Janni, J. D. Klein and K. M. Spencer, *Anal. Chem.*, 2000, **72**, 5834–5840.

23 S. Gura, M. Madmon, N. Tzanani, R. Barak, I. Shacht and S. Dagan, *Anal. Methods*, 2017, **9**, 393–401.

24 V. Heleg-Shabtai, H. Sharabi, A. Zaltsman, I. Ron and A. Pevzner, *Analyst*, 2020, **145**, 6334–6341.

25 A. Shiohara, Y. Wang and L. M. Liz-Marzán, *J. Photochem. Photobiol., C*, 2014, **21**, 2–25.

26 B. Stuart, *Forensic Analytical Techniques*, John Wiley & Sons, Ltd, Chichester, UK, 2012.

27 D. Chambers, C. Brackett and D. O. Sparkman, *Perspectives on Pentaerythritol Tetranitrate (PETN) Decomposition*, Livermore, CA (United States), 2002.

28 S. E. J. Bell and N. M. S. Sirimuthu, *Chem. Soc. Rev.*, 2008, **37**, 1012–1024.

29 L. Wang, M. Ghosh and S. A. Asher, *Appl. Spectrosc.*, 2012, **66**(9), 1013–1021.

30 L. Nagli, M. Gaft, Y. Fleger and M. Rosenbluh, *Opt. Mater.*, 2008, **30**, 1747–1754.

31 S. Li, Q. Li, K. Wang, M. Zhou, X. Huang, J. Liu, K. Yang, B. Liu, T. Cui, G. Zou and B. Zou, *J. Phys. Chem. C*, 2013, **117**, 152–159.

32 J. Almog, G. Burda, Y. Shloosh, S. Abramovich-Bar, E. Wolf and T. Tamiri, *J. Forensic Sci.*, 2007, **52**, 1284–1290.

33 K. R. Lynn, *J. Phys. Chem.*, 1965, **69**, 687–689.

34 A. Sumayya, C. Y. Panicker, H. Varghese and B. Harikumar, *Rasayan J. Chem.*, 2008, **1**, 548–555.

35 J. De Gelder, K. De Gussem, P. Vandenabeele and L. Moens, *J. Raman Spectrosc.*, 2007, **38**, 1133–1147.

36 A. Parameswari, S. Premkumar, R. Premkumar and A. Milton Franklin Benial, *J. Mol. Struct.*, 2016, **1116**, 180–187.

37 F. Zapata, M. López-López and C. García-Ruiz, *Appl. Spectrosc. Rev.*, 2016, **51**, 227–262.

38 P. M. Fierro-Mercado and S. P. Hernández-Rivera, *Int. J. Spectrosc.*, 2012, **2012**, 1–7.

39 M. E. Walsh, T. F. Jenkins and P. G. Thorne, *J. Energ. Mater.*, 1995, **13**, 357–383.

40 K. M. Spencer, J. M. Sylvia, J. A. Janni and J. D. Klein, in *Detection and Remediation Technologies for Mines and Minelike Targets IV*, ed. A. C. Dubey, J. F. Harvey, J. T. Broach and R. E. Dugan, SPIE, 1999, vol. 3710, p. 373.

41 R. Ravikrishna, K. T. Valsaraj, C. B. Price, J. M. Brannon, C. A. Hayes and S. L. Yost, *J. Air Waste Manage. Assoc.*, 2004, **54**, 1525–1533.

42 H. Östmark, S. Wallin and H. G. Ang, *Propellants, Explos., Pyrotech.*, 2012, **37**, 12–23.